Acta Crystallographica Section B
Structural Science
ISSN 0108-7681

Atomic thermal motions studied by variable-temperature X-ray diffraction and related to non-linear optical properties of crystalline *meta*-dinitrobenzene

Grażyna Wójcik,* Izabela Mossakowska, Jolanta Holband and Wojciech Bartkowiak

Institute of Physical and Theoretical Chemistry, Wrocław University of Technology, Wyb. Wyspiańskiego 27, 50-370 Wrocław, Poland

Correspondence e-mail: wojcik@kchf.ch.pwr.wroc.pl

Received 21 January 2002
Accepted 19 August 2002

The *meta*-dinitrobenzene crystal structure has been determined at five temperatures in the 100–300 K temperature range. The thermal expansion coefficients have been calculated from the temperature variation of the lattice parameters. Rigid-body motion analysis with allowance for large-amplitude internal motions provided the **T**, **L** and **S** tensors' values at the temperatures studied and was used to characterize the torsional motion of two nitro groups in the molecule. Frequencies of the translational and librational modes and of the torsional modes of the nitro groups have been compared with the wave numbers at the maximum of bands in the low-frequency Raman and IR spectra. *Ab initio* calculations were performed in order to assess the contribution from large-amplitude internal motions to the static first-order hyperpolarizability of the *m*-dinitrobenzene molecule.

1. Introduction.

Variable-temperature crystal-structure studies of several organic crystals that exhibit non-linear optical properties have recently been performed by us. In particular we have studied *m*-nitroaniline (Wójcik & Holband, 2001), 4-isopropylphenol (Wójcik & Holband, 2002) and two polymorphic forms of *m*-nitrophenol (Wójcik & Holband, 2003). These small-molecule compounds seem to be good candidates for an investigation aiming to advance discussion on the relationship between structure and molecular interactions *versus* non-linear optical properties. Extensive variable-temperature spectroscopic studies of the materials, including IR and Raman scattering spectra, solid-state NMR, dielectric relaxation and inelastic neutron scattering, had previously been completed in our laboratory (Szostak, 1979, 1982, 1988; Szostak *et al.*, 1994, 1995; Szostak, Wójcik *et al.*, 1998; Szostak, Kozankiewicz *et al.*, 1998; Giermańska *et al.*, 1990; Wójcik *et al.*, 1991, 1992, 1999). The results concerning the thermal behaviour of the materials and the low-frequency vibrations remain in line with the results of variable-temperature X-ray diffraction experiments (Wójcik & Holband, 2001, 2002). The three compounds mentioned have many common structural features such as a substituted benzene ring, intermolecular hydrogen bonds, a packing consisting of molecular chains and an intermolecular charge transfer along the molecular string coupled with some molecular librations of large amplitudes (Wójcik & Holband, 2001, 2002; Szostak *et al.*, 1995).

Meta-dinitrobenzene (hereafter called mDNB) was the next material in the series to arouse our interest. It shows second-harmonic generation with an efficiency 1–5 times greater than KDP, a standard non-linear material (Southgate & Hall, 1972). mDNB, however, differs from the previously studied materials because it does not contain strong or intermediate hydrogen

Table 1
Experimental details.

	100 K	130 K	160 K	200 K	300 K
Crystal data					
Chemical formula	$C_6H_4N_2O_4$	$C_6H_4N_2O_4$	$C_6H_4N_2O_4$	$C_6H_4N_2O_4$	$C_6H_4N_2O_4$
Chemical formula weight	168.11	168.11	168.11	168.11	168.11
Cell setting, space group	Orthorhombic, $Pna2_1$	Orthorhombic, $Pna2_1$	Orthorhombic, $Pna2_1$	Orthorhombic, $Pna2_1$	Orthorhombic, $Pna2_1$
a, b, c (Å)	14.024 (2), 13.182 (2), 3.677 (1)	14.040 (4), 13.208 (4), 3.694 (1)	14.052 (4), 13.224 (4), 3.714 (1)	14.069 (2), 13.245 (2), 3.738 (1)	14.084 (4), 13.292 (4), 3.802 (1)
V (Å^3)	679.7 (2)	685.0 (3)	690.1 (3)	696.6 (2)	711.8 (3)
Z	4	4	4	4	4
D_x (Mg m^{-3})	1.643	1.630	1.618	1.603	1.569
Radiation type	Mo $K\alpha$	Mo $K\alpha$	Mo $K\alpha$	Mo $K\alpha$	Mo $K\alpha$
No. of reflections for cell parameters	1717	826	958	1607	739
θ range (°)	3.345–22.626	3.336–17.260	3.334–16.759	3.345–24.195	3.334–18.722
μ (mm^{-1})	0.142	0.141	0.140	0.138	0.135
Crystal form, colour	Prism, colourless	Prism, colourless	Prism, colourless	Prism, colourless	Prism, colourless
Crystal size (mm)	0.72 × 0.33 × 0.23	0.72 × 0.33 × 0.23	0.72 × 0.33 × 0.23	0.72 × 0.33 × 0.23	0.72 × 0.33 × 0.23
Data collection					
Diffractometer	KUMA Diffraction KM4CCD	Kuma Diffraction KM4CCD	KUMA Diffraction KM4CCD	KUMA Diffraction KM4CCD	KUMA Difffraction KM4CCD
Data collection method	ω scans	ω scans	ω scans	ω scans	ω scans
No. of measured, independent and observed reflections	5634, 1448, 1388	5088, 1422, 1322	3208, 1212, 1077	5386, 1475, 1330	5456, 1486, 1177
Criterion for observed reflections	$I > 2\sigma(I)$	$I > 2\sigma(I)$	$I > 2\sigma(I)$	$I > 2\sigma(I)$	$I > 2\sigma(I)$
R_{int}	0.0686	0.0589	0.1000	0.0680	0.0411
θ_{max} (°)	31.22	31.15	31.19	31.23	31.13
Range of h, k, l	$-20 \rightarrow h \rightarrow 20$ $-19 \rightarrow k \rightarrow 18$ $-5 \rightarrow l \rightarrow 3$	$-20 \rightarrow h \rightarrow 20$ $-19 \rightarrow k \rightarrow 18$ $-5 \rightarrow l \rightarrow 3$	$-18 \rightarrow h \rightarrow 20$ $-18 \rightarrow k \rightarrow 15$ $-5 \rightarrow l \rightarrow 2$	$-20 \rightarrow h \rightarrow 20$ $-19 \rightarrow k \rightarrow 18$ $-3 \rightarrow l \rightarrow 5$	$-20 \rightarrow h \rightarrow 20$ $-19 \rightarrow k \rightarrow 19$ $-3 \rightarrow l \rightarrow 5$
No. frames	552	552	552	552	552
Scan width (°)	0.8	0.8	0.8	0.8	0.8
Time of exposure (°)	10	10	10	10	10
Refinement					
Refinement on	F^2	F^2	F^2	F^2	F^2
$R[F^2>2\sigma(F^2)]$, $wR(F^2)$, S	0.0412, 0.1232, 1.163	0.0561, 0.1423, 1.183	0.054, 0.1554, 1.167	0.054, 0.1456, 1.045	0.0797, 0.2379, 1.203
No. of reflections and parameters used in refinement	1448, 109	1422, 109	1212, 109	1475, 109	1486, 109
H-atom treatment	Mixed	Mixed	Mixed	Mixed	Mixed
Weighting scheme	$w = 1/[\sigma^2(F_o^2) + (0.0769P)^2 + 0.0678P]$ where $P = (F_o^2 + 2F_c^2)/3$	$w = 1/[\sigma^2(F_o^2) + (0.0504P)^2 + 0.5159P]$ where $P = (F_o^2 + 2F_c^2)/3$	$w = 1/[\sigma^2(F_o^2) + (0.0717P)^2 + 0.2515P]$ where $P = (F_o^2 + 2F_c^2)/3$	$w = 1/[\sigma^2(F_o^2) + (0.0747P)^2 + 0.2161P]$ where $P = (F_o^2 + 2F_c^2)/3$	$w = 1/[\sigma^2(F_o^2) + (0.1144P)^2 + 0.1108P]$ where $P = (F_o^2 + 2F_c^2)/3$
$(\Delta/\sigma)_{max}$	0.000	0.000	0.000	0.000	0.000
$\Delta\rho_{max}$, $\Delta\rho_{min}$ (e Å^{-3})	0.277, −0.318	0.315, −0.291	0.292, −0.319	0.21, −0.224	0.246, −0.331

Computer programs used: *KUMA KM4CCD* software (KUMA Diffraction, 1999); *SHELXL*97 (Sheldrick, 1997); *SHELXS*97 (Sheldrick, 1990).

bonds and does not pack in strings. Instead the crystal structure shows a planar packing of molecules and surprisingly short intermolecular O···O contacts along the polar axis (Trotter, 1961). We chose this material since its molecular packing and intermolecular interactions provided new aspects in our investigations of the structure *versus* property relationship. The room-temperature crystal structure of mDNB was thoroughly studied by Trotter in the 1960s (Trotter, 1961). He also performed rigid-body analysis of the C atoms from the aromatic ring of the mDNB molecule (Trotter, 1966). His results report very large atomic displacement parameters at room temperature.

Our results concerning the crystal structures at five temperatures in the 100–300 K temperature range, thermal expansion and rigid-body analysis of the anisotropic displacement parameters, including correlation of the torsional vibrations of the nitro groups, are discussed below. They point to very large amplitudes of the nitro groups' vibrations, which increase strongly with temperature. The contribution of these vibrations to the second-order non-linear responses of the

material seems to be relevant. To check this assumption we performed quantum-chemical calculations of the vibrational and electronic components of the static first-order hyperpolarizability of the mDNB molecule.

2. Experimental

Commercial mDNB was further purified by multiple-zone melting. Single-crystal specimens were grown from a methanol solution. They had a pale yellow colour and melted at 364 K. Preliminary differential scanning calorimetry measurements did not show any thermodynamic transition from 120 K up to the melting point.

X-ray diffraction measurements were performed on a KUMA Diffraction four-circle automatic diffractometer equipped with an area detector and an Oxford Cryosystem cooling unit. Mo $K\alpha$ radiation ($\lambda = 0.71073$ Å) was used. The measurements were performed at five temperatures: 100, 130, 160, 200 and 300 K. The precision of the temperature stability was 0.1 K. During the data collection, ω scans were performed. No absorption corrections were used. Data reductions were performed with *KUMA KM4CCD* software (Kuma Diffraction, 1999). The structures were solved by direct methods (Sheldrick, 1990) and refined by least-squares methods with programs from the *SHELXL*97 package (Sheldrick, 1997). Atomic scattering factors were taken from the *International Tables for Crystallography* (1992, Vol. C, Tables 4.2.6.8 and 6.1.1.4). The H atoms were found by the riding model and refined isotropically. Other details of the data collection and the refinement are shown in Table 1.[1] The rigid-body analysis (Cruickshank, 1956; Schomaker & Trueblood, 1968; Dunitz & White, 1973), including the correlation of the internal motion of the non-rigidly attached rigid groups (Dunitz *et al.*, 1988; Schomaker & Trueblood, 1998), was performed with *THMA*11 (Trueblood, 1978; Farrugia, 1999).

The *ab initio* Hartree–Fock (HF) method was used to study the vibrational $\beta^{v}(0)$ and electronic $\beta^{e}(0)$ components of the static first-order hyperpolarizability of the mDNB molecule. The calculations were carried out with *GAUSSIAN*94 (Frisch *et al.*, 1995). The standard 6-31G basis set was used for all calculations. The geometry was optimized without symmetry restrictions by the gradient procedure at the HF level. It was found that the 6-31G basis set offers a reliable tool for the behaviour of β for various compounds (Champagne, 1996; Champagne & Kirtman, 1999; Jacquemin *et al.*, 1997).

The $\beta^{e}(0)$ component was calculated by applying the coupled perturbed Hartree–Fock (CPHF) theory according to the methodology of Hurst (Hurst *et al.*, 1988). The double harmonic oscillator approximation was used to evaluate the static vibrational hyperpolarizability $[\beta^{v}(0)]$ (Bishop & Kirtman, 1991, 1992; Bishop, 1998). This approach is based on the perturbation-theoretical method of Bishop & Kirtman (1991, 1992). In this method, the expression

$$\beta_{\zeta\eta\xi}(0) = (\mu\alpha)^{0,0} = \sum_k \omega_k^{-2}\left[(\delta\mu_\zeta/\delta Q_k)(\delta\alpha_{\eta\xi}/\delta Q_k)_0 + (\delta\mu_\eta/\delta Q_k)(\delta\alpha_{\zeta\xi}/\delta Q_k)_0 + (\delta\mu_\xi/\delta Q_k)(\delta\alpha_{\zeta\eta}/\delta Q_k)_0\right] \quad (1)$$

is used for the individual components of the $\beta^{v}(0)$ tensor. The summation in (1) runs over $3N - 6$ (where N is the number of atoms in the molecule) vibrational normal modes (Q_k) of frequencies ω_k, which are evaluated at the equilibrium geometry. The symbols μ and α denote the molecular dipole moment and the molecular polarizability, respectively. The subscripts ζ, η and ξ refer to the molecular Cartesian coordinates x, y and z. The axes are shown in Fig. 1. The above method is also known as the sum-over-modes (SOM) procedure (Champagne, 1996). It should be noted that (1) was independently obtained based on the semiclassical model by Zerbi (Castiglioni *et al.*, 1992). The SOM procedure was implemented in *GAUSSIAN*94 (Bartkowiak & Misiaszek, 2000).

The vector component (2) of the first-order hyperpolarizability tensor was used to compare $\beta^{v}(0)$ and $\beta^{e}(0)$ (Champagne & Kirtman, 1999; Champagne, 1996; Bishop, 1998; Willetts *et al.*, 1992):

$$\beta_\mu = \sum_\zeta (\mu_\zeta \beta_\zeta / |\mu|), \quad (2)$$

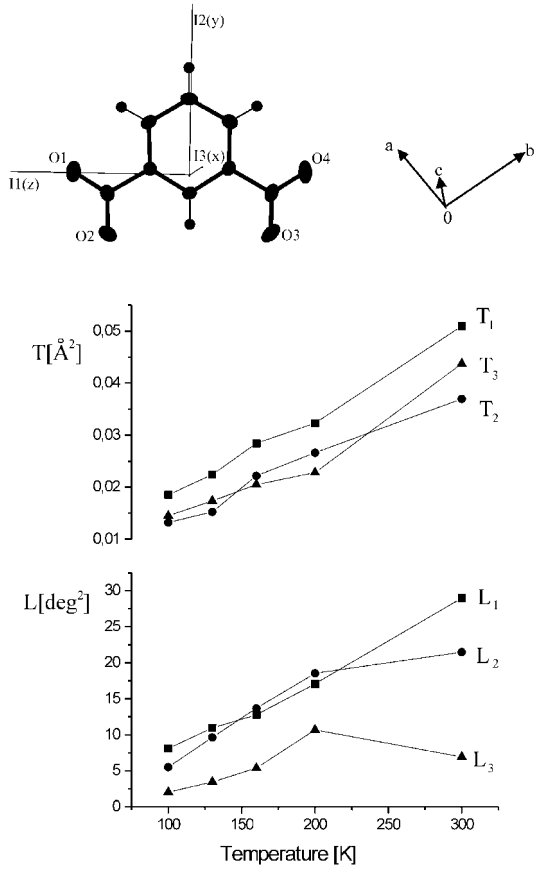

Figure 1
The thermal evolution of the principal values of the translation and libration tensors. Solid lines serve as guides to the eye. The inertial axes I_1, I_2 and I_3 of the molecule are shown with respect to the crystallographic a, b, c axes. Also the molecular axes x, y, z used in *GAUSSIAN*94 are shown. For more details see the text.

[1] Supplementary data for this paper are available from the IUCr electronic archives (Reference: NS0009). Services for accessing these data are described at the back of the journal.

Table 2
Short intermolecular distances in the *m*-dinitrobenzene crystal at 100 and 300 K.

	100 K	300 K
O1^{vii}···H4^{i}	3.050	3.129
O1^{vii}···H5^{vi}	2.533	2.633
O1^{vii}···H5^{i}	2.959	3.104
O2^{vii}···H2^{iii}	2.763	2.896
O2^{vii}···H2^{v}	2.613	2.689
O2^{vii}···H5^{i}	2.912	3.009
O3^{v}···H5^{i}	2.924	2.992
O3^{iii}···H6^{i}	3.014	3.110
O3^{v}···H6^{i}	2.465	2.555
O4^{iv}···H4^{iii}	2.581	2.635
O4^{iv}···H4^{v}	3.366	3.541
O4^{iv}···H6^{ii}	2.903	3.047
O1^{iii}···O2^{v}	3.016	3.146
O2^{iii}···O2^{vii}	3.110	3.185
O3^{v}···O4^{iii}	3.261	3.491
O4^{iii}···O4^{iv}	3.280	3.421

(i) x, y, z; (ii) $-x, -y, z+\frac{1}{2}$; (iii) $x+\frac{1}{2}, -y, z+\frac{1}{2}$; (iv) $-x+\frac{1}{2}, y+\frac{1}{2}, z+\frac{1}{2}$; (v) $x+\frac{1}{2}, -y, z+1$; (vi) $x, y, z+\frac{3}{2}$; (vii) $-x+\frac{1}{2}, y+\frac{3}{2}, z+\frac{1}{2}$.

where $\beta_\eta = \sum_\eta(\beta_{\zeta\eta\eta})$.

The Taylor series convention (so-called T convention) for theoretically determined values of the hyperpolarizability was adopted in this work (Willetts *et al.*, 1992).

3. Results and discussion

3.1. Molecular packing

The room-temperature mDNB crystal structure determined by us is generally consistent with the one reported by Trotter (1961, 1966). However, we determined the structure in the $Pna2_1$ space group rather than the $Pbn2_1$ group reported by Trotter, and thus our *a*, *b*, *c* lattice parameters correspond to the *b*, *a*, *c* parameters of Trotter. In the crystal the molecules are planar, except for the O atoms, which are twisted from the molecular plane by about 10° for O_1 (down) and O_2 (up) and by about 12° for O_3 (up) and O_4 (down) at 300 K. The conformation of two nitro groups in the molecule changes slightly with temperature, and the respective angles at 100 K are equal to about 12° and 15°. Fig. 2 shows the mDNB molecule with atom numbering. The two nitro groups are not in a fully equivalent environment, and this is clearly seen when we discuss their short intermolecular contacts in the crystal (see Table 2).

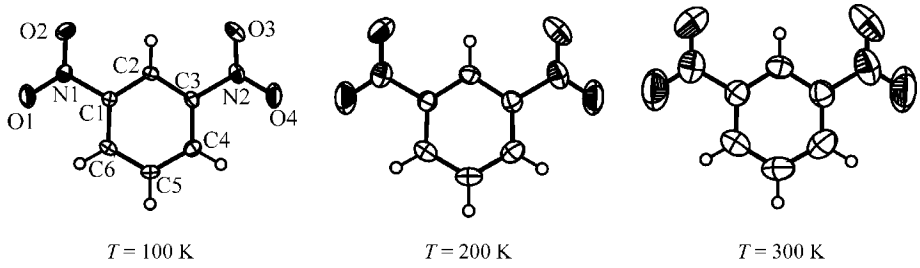

Figure 2
*ORTEP*3 (Farrugia, 1999) view of the *m*-dinitrobenzene molecule with atom numbering and the ellipsoids of atomic displacements drawn at the 50% probability level at 100, 200 and 300 K.

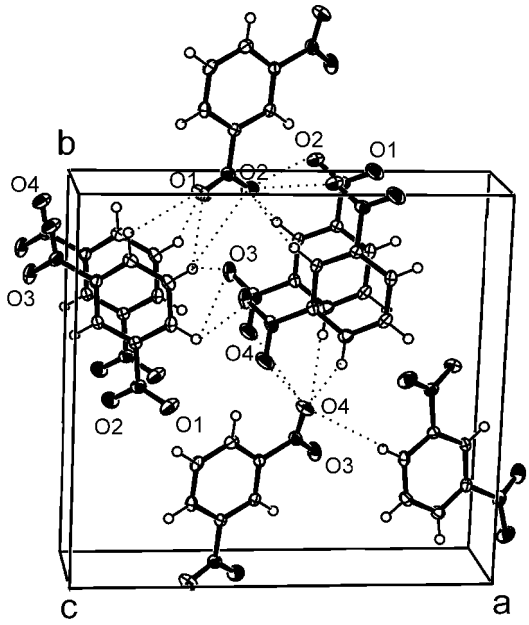

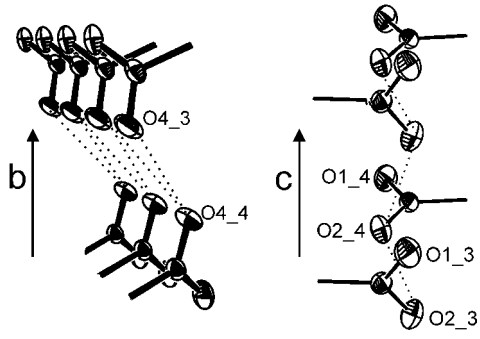

Figure 3
Short intermolecular contacts in the *m*-dinitrobenzene crystal.

The positional and displacement parameters determined at five temperatures have been deposited. Fig. 2 shows the mDNB molecule with the anisotropic displacement ellipsoids at three temperatures from the range covered by the experiment. The molecules in the crystal are involved in numerous weak CH···O hydrogen bonds, which evidently stabilize their planar arrangement on the *ab* plane. The O atoms twisted from the molecular planes show mutual short intermolecular contacts along the polar *c* axis. All short intermolecular contacts in the crystal at 100 K and 300 K are listed in Table 2 and shown in Fig. 3.

3.2. Influence of temperature

Temperature variation does not influence bond lengths and angles very much. Apart from the O atoms, the molecule remains planar within a 2° deviation. The torsional angles of the two nitro groups decrease their values

Table 3
Principal thermal-expansion coefficients (deg^{-1}) of *m*-dinitrobenzene at 100 and 300 K.

The errors on the coefficients are estimated as equal to about 1×10^{-6} deg^{-1}. $\alpha_1||a, \alpha_2||b, \alpha_3||c$.

	100 K	300 K
α_1	4.14×10^{-5}	0.16×10^{-5}
α_2	5.45×10^{-5}	2.71×10^{-5}
α_3	1.38×10^{-4}	2.58×10^{-4}

from 12° and 15° at 100 K to 10° and 12° at 300 K. The temperature increase influences mainly the N—O bond lengths owing to the increasing torsional amplitudes of the nitro groups. The relative shortening of the bonds between 100 K and 300 K amounts to about 1%. Table 2 reports the elongation of short intermolecular contacts with increasing temperature. Nevertheless it is obvious that they do not change essentially.

Taking into account the large displacement amplitudes of the O atoms, we assumed that a considerable thermal expansion of the crystal occurred. The relative variation of the lattice parameters with temperature is shown in Fig. 4. The thermal expansion coefficients along the crystallographic axes, α_1, α_2, α_3, were calculated from the non-linear fits of the relative elongation of the lattice parameters as a function of temperature increase. In the orthorhombic crystallographic system they correspond to the principal coefficients of the thermal-expansion tensor. The coefficients at 100 K and 300 K, *i.e.* at temperatures on the limits of the range covered by the experiment, are reported in Table 3. The largest expansion occurs along the *c* axis while the expansion along the two other crystallographic axes are about two orders of magnitude smaller. The thermal expansion reflects the interactions occurring in the mDNB crystal, which are highly anharmonic along the *c* axis.

Following our recent rigid-body studies of *m*-nitroaniline (Wójcik & Holband, 2001) and the rigid-body analysis of the C atoms' displacement parameters at room temperature

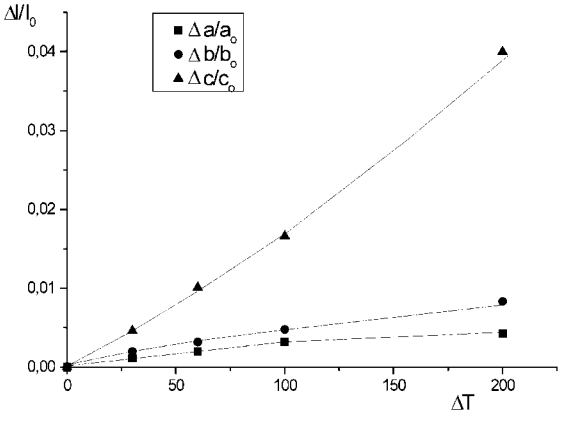

Figure 4
The relative elongation of the *m*-dinitrobenzene lattice parameters as a function of temperature increase. The lines are the non-linear fit to the experimental points.

Table 4
The values of the rigid-body **T** (Å^2), **L** (deg^2) and **S** (rad Å) tensors at 100 and 300 K in the inertial coordinate system.

		100 K	300 K
T	T^{11}	0.01794	0.04994
	T^{12}	−0.00163	−0.00326
	T^{13}	−0.00014	0.00079
	T^{22}	0.01390	0.04047
	T^{23}	0.00043	0.00319
	T^{33}	0.01441	0.04126
L	L^{11}	5.486	21.455
	L^{12}	0.349	0.545
	L^{13}	−0.167	0.116
	L^{22}	2.258	7.506
	L^{23}	−1.040	−3.470
	L^{33}	7.908	28.433
S	S^{11}	−0.00028	−0.00033
	S^{12}	−0.00030	−0.00006
	S^{13}	−0.00056	−0.00136
	S^{21}	−0.00069	−0.00116
	S^{22}	0.00065	0.00148
	S^{23}	0.00023	0.00137
	S^{31}	0.00040	0.00187
	S^{32}	−0.00058	−0.00221
	S^{33}	−0.00038	−0.00182
wR†		0.063	0.053

† $wR = \left[\sum w(U_o^{ij} - U_c^{ij})^2 / \sum w U_o^{ij2}\right]^{1/2}$; $w = \sigma\left[\langle U_o^{ij}\rangle\right]^{-2}$.

performed by Trotter (Trotter, 1966), we used this method to analyse the anisotropic displacement parameters of all non-H atoms of the mDNB molecule. The correlation with the large-amplitude internal motion included in *THMA*11 (Trueblood, 1978; Farrugia, 1999) turned out to be crucial. Table 4 reports the values of **T** (translation), **L** (libration) and **S** (correlation between molecular translations and librations in the case of a non-centrosymmetric molecule) tensors in the inertial axes frame calculated at 100 K and 300 K. Fig. 1 shows the variation of the principal values of the **T** and **L** tensors with temperature. This dependence is worthy of some comment. The T_1, T_2 and T_3 principal values are similar and slightly smaller than in the case of *m*-nitroaniline (Wójcik & Holband, 2001) and 4-isopropylphenol (Wójcik & Holband, 2002). The libration-tensor principal values are far smaller than in 4-isopropylphenol and smaller than in *m*-nitroaniline. This comparison reflects the difference in the molecular packings of mDNB and the other crystals. The libration amplitude L_3, which occurs roughly about the I_2 inertial axis, is distinctly smaller than the two other principal librations, L_1 and L_2, which occur roughly about the two other inertial axes (I_3 and I_1, respectively). The maximum of the L_3 dependence on temperature around 200 K and a smaller one for the L_2 dependence on temperature seem to be related to the strong increase of the nitro groups' torsion amplitudes at the same temperature (see Fig. 5). The amplitudes of the considered motions are directed along the *c* axis, that is, the direction of the largest thermal expansion.

Our rigid-body analysis results indicate that the large anisotropic displacement parameters originate more from the nitro groups' internal motions than from the molecular

translations and librations. The mean-square amplitudes of the overall motions about the two torsion axes and the amplitudes of the molecular librations about the same axes, calculated at five temperatures, are shown in Fig. 5. It follows that the amplitudes of the nitro-group torsions are large at 100 K and grow enormously with temperature. They are thus crucial for understanding the thermal behaviour of the mDNB crystal. It is not clear whether the discrepancies between the two amplitudes of the overall motions at 200 K and 300 K reflect the difference in the two nitro groups' environments or whether the approximation to the average value shown in Fig. 5 is plausible for both nitro groups' motions.

3.3. Molecular vibrations from the rigid-body and *ab initio* calculations

Normal modes were calculated from the molecular-motion amplitudes within the harmonic approximation. The frequency values are listed in Table 5. To some extent they may be compared with the frequencies from the low-frequency Raman and IR spectra. Nevertheless one should remember that the normal modes from diffraction represent

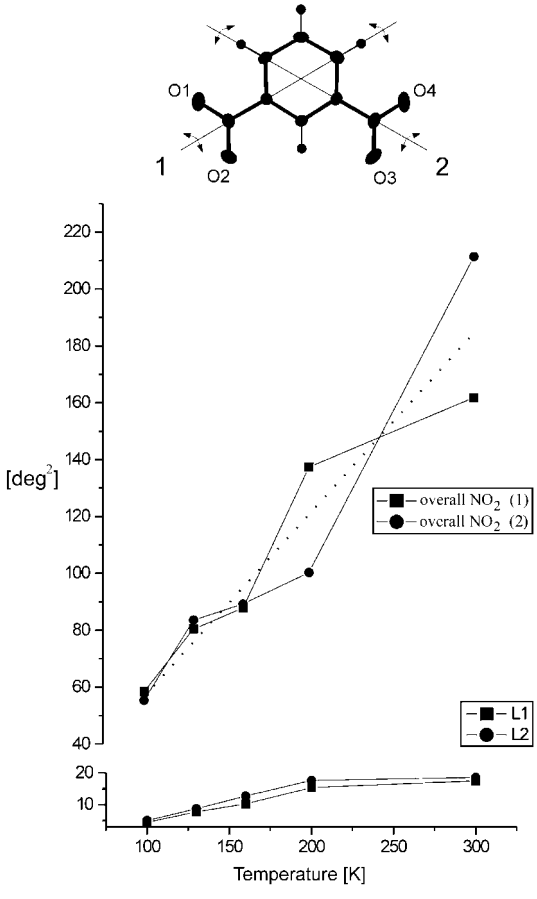

Figure 5
The temperature dependence of the amplitudes of the overall (upper curves) and librational (bottom curves) motions of the nitro groups about the torsion axes. Solid lines serve as guides to the eye. The broken line corresponds to the least-squares approximation of both overall amplitudes to one value. The torsion axes are shown with respect to the mDNB molecule. For more details see the text.

Table 5
The normal modes and internal torsion (τ) frequencies from the rigid-body analysis (this work, average values for all temperatures), the frequencies at the maximum of bands in the low-frequency Raman scattering and IR spectra of crystalline mDNB (Bobrov *et al.*, 1974; average values for all polarizations), and the low-frequency normal modes from *ab initio* calculations (this work).

Rigid-body analysis	IR	Raman	*GAUSSIAN*94
27 T_1	28	19	
		24	
30 T_2	32	31	
32 T_3			
34 L_1	40	38	
56 L_2		56	
70 L_3	78	79	
		105	
63 τ_1		61 τ	50 τ
64 τ_2			57 τ
	162	163	176
			178
		198	221

average values of frequencies from the first Brillouin zone (Bürgi, 1995) while the frequencies from the optical spectra correspond to the centre of the Brillouin zone. The frequencies of lattice vibrations from optical spectra are not molecular normal modes, but their combinations result from crystal symmetry and the number of molecules in a unit cell (Turrell, 1972). Extensive IR and Raman studies of mDNB in different environments (solution, solid, crystal) were performed by Bobrov and co-workers in the 1970s (Bobrov *et al.*, 1974). The polarized IR and Raman spectra of crystalline mDNB provided the values of lattice frequencies that occur between 19 and 105 cm^{-1}. Taking into account the difficulties of comparing our frequency values calculated from the diffraction data with the frequency values from the optical spectra, we considered the normal-mode frequencies from X-ray diffraction averaged over all temperatures measured and the frequencies from the optical spectra averaged for all polarizations. The comparison is reported in Table 5.

Three translation frequencies (27, 30 and 32 cm^{-1}) and three libration frequencies (34, 56 and 70 cm^{-1}) remain relatively consistent with the frequencies of lattice vibrations reported by Bobrov (Bobrov *et al.*, 1974) and cited in Table 5. According to the group-theory analysis (Turrell, 1972) for the mDNB crystal (C_{2v} point group, four molecules in the unit cell) we expect $24 - 3 = 21$ lattice vibrations that are active in both Raman and IR spectra. Bobrov observed fewer than half as many bands in the lattice-vibration spectral range, probably owing to the degeneration of some frequencies. The frequency of 61 cm^{-1} assigned by Bobrov to the internal torsion of nitro groups remains in excellent agreement with the values 63 and 64 cm^{-1} calculated within the rigid-body analysis as the frequencies of the torsional motions of the nitro groups. It also means that the two nitro groups are energetically almost equivalent in spite of slightly different environments in the crystal. Estimated from the torsion amplitudes, the energetic barrier to the torsion is equal to about 28 kJ mole^{-1} at about 100 K and 25 kJ mole^{-1} at 300 K. The force constants for the

two torsional vibrations are about 17 and 15 kJ mole^{-1} deg^2 at 100 and 300 K, respectively.

The *ab initio* calculations provided the normal modes of the isolated mDNB molecule. The lowest frequencies (50, 57, 176, 178 and 221 cm^{-1}) are cited in Table 5. The first three vibrations are connected to the nitro groups' torsional motions. The mode 50 cm^{-1} is inactive in the IR spectrum, while the modes 57 and 176 cm^{-1} are observed in the IR and Raman spectra. These two low-frequency internal modes significantly contribute to the static vibrational first-order hyperpolarizability. The vibrational first-order hyperpolarizability [$\beta^{v}_{\mu}(0)$] is equal to -5.17×10^{-30} s.u. and is about eight times larger than the electronic first-order hyperpolarizability [$\beta^{e}_{\mu}(0)$, equal to 0.67×10^{-30} s.u.]. In our calculations, the molecular plane is located in the (yz) plane with the molecular dipole moment along the y axis (the axes are shown in Fig. 1). The dipole moment is equal to 5.48 D and may be compared with the dipole moments of the *m*-nitroaniline molecule (6.58 D) and the *m*-nitrophenol molecule (6.84 D) (Szostak *et al.*, 1998; Wójcik *et al.*, 1996). The major contribution to $\beta^{v}_{\mu}(0)$ comes from components β^{v}_{yyy}, β^{v}_{yxx} and β^{v}_{yzz}. The calculated absolute values of these components are equal to -0.96×10^{-31}, 1.82×10^{-30} and -6.89×10^{-30} s.u., respectively. The normal mode with frequency of 57 cm^{-1} gives about 90% of the total value of the largest component (β^{v}_{yzz}).

4. Conclusions

As far as molecular librations are concerned, the results of the rigid-body analysis of the mDNB crystal structure remain contrary to our previous results for other nitrobenzene derivatives, *i.e.* *m*-nitroaniline (Wójcik & Holband, 2001) and *m*-nitrophenol (Wójcik & Holband, 2003). This inconsistency originates from the planar molecular packing in the mDNB crystal, which is different from the molecular chains of hydrogen-bonded molecules in the other crystals. The most pronounced motion in these crystals appeared to be the molecular libration about the axis directed along the intermolecular hydrogen bonds.

The most important motion in the crystalline mDNB was the internal torsion of the two nitro groups. These large-amplitude vibrations result in a large thermal expansion along the c axis. The O$\cdots$O interactions along the c axis seem to result in some charge transfer coupled with the nitro groups' large-amplitude vibrations. Results from our *ab initio* calculations indicate that the non-linear optical properties of the isolated mDNB molecule have a dominant contribution from the torsional vibrations of the nitro groups. The intermolecular interactions in the crystal may enhance the properties in such a way that the short intermolecular distances between the O atoms along the c axis together with their large amplitudes of torsion result in some cooperativity and even a tuning of the motions.

This work was sponsored by the Polish National Committee for Scientific Research under the Wroclaw University of Technology statutory funds.

References

Bartkowiak, W. & Misiaszek, T. (2000). *Chem Phys.* **261**, 353–357.
Bishop, D. M. (1998). *Adv. Chem. Phys.* **104**, 1–53.
Bishop, D. M. & Kirtman, B. (1991). *J. Chem. Phys.* **95**, 2646–2658.
Bishop, D. M. & Kirtman, B. (1992). *J. Chem. Phys.* **97**, 5255–5256.
Bobrov, A. V., Mathieu, J. P. & Poulet, H. (1974). *J. Raman Spectrosc.* **2**, 381–389.
Bürgi, H.-B. (1995). *Acta Cryst.* B**51**, 571–579.
Castiglioni, C., Gussoni, M., Del Zoppo, M. & Zerbi, G. (1992). *Solid State Commun.* **82**, 13–17.
Champagne, B. (1996). *Chem. Phys. Lett.* **261**, 57–65.
Champagne, B. & Kirtman, B. (1999). *Chem. Phys.* **245**, 213–226.
Cruickshank, D. W. J. (1956). *Acta Cryst.* **9**, 754–756.
Dunitz, J. D., Maverick, E. F. & Trueblood, K. N. (1988). *Angew. Chem. Int. Ed. Engl.* **27**, 880–895.
Dunitz, J. D. & White, D. N. J. (1973). *Acta Cryst.* A**29**, 93–94.
Farrugia, L. (1999). *J. Appl. Cryst.* **32**, 837–838.
Frisch, M. J. *et al.* (1995). *GAUSSIAN*94. Revision A.1. Gaussian Inc., Pittsburgh, PA, USA.
Giermańska, J., Wójcik, G. & Szostak, M. M. (1990). *J. Raman Spectrosc.* **21**, 479–489.
Hurst, G. J. B., Dupuis, M. & Clementi, E. (1988). *J. Chem. Phys.* **89**, 385–395.
Jacquemin, D., Champagne, B. & Andre, J.-M. (1997). *Int. J. Quantum Chem.* **65**, 679–688.
Kuma Diffraction (1999). *Kuma KM4CCD Software.* Version 1.61. Kuma Diffraction, Wrocław, Poland.
Schomaker, V. & Trueblood, K. N. (1968). *Acta Cryst.* B**24**, 63–76.
Schomaker, V. & Trueblood, K. N. (1998). *Acta Cryst.* B**54**, 507–514.
Sheldrick, G. M. (1990). *Acta Cryst.* A**46**, 467–473.
Sheldrick, G. M. (1997). *SHELXL*97. University of Göttingen, Germany.
Southgate, P. D. & Hall, D. S. (1972). *J. Appl. Phys.* **43**, 2765–2771.
Szostak, M. M. (1979). *J. Raman Spectrosc.* **8**, 43–49.
Szostak, M. M. (1982). *J. Raman Spectrosc.* **12**, 228–233.
Szostak, M. M. (1988). *Chem. Phys.* **121**, 449–456.
Szostak, M. M., Kozankiewicz, B., Wójcik, G. & Lipiński, J. (1998). *J. Chem. Soc. Faraday Trans.* **94**, 3241–3245.
Szostak, M. M., Le Calve, N., Romain, F. & Pasquier, B. (1994). *Chem. Phys.* **187**, 373–380.
Szostak, M. M., Misiaszek, T., Roszak, S., Rankin, J. G. & Czernuszewicz, R. S. (1995). *J. Phys. Chem.* **99**, 14992–15003.
Szostak, M. M., Wójcik, G., Gallier, J., Berteault, M., Freundlich, P. & Kołodziej, H. A. (1998). *Chem. Phys.* **229**, 275–284.
Trotter, J. (1961). *Acta Cryst.* **14**, 244–250.
Trotter, J. (1966). *Acta Cryst.* **21**, 285–288.
Trueblood, K. N. (1978). *Acta Cryst.* A**34**, 950–954.
Turrell, G. (1972). *Infrared and Raman Spectra of Crystals.* London/New York: Academic Press.
Willetts, A., Rice, J. E., Burland, D. M. & Shelton, D. P. (1992). *J. Chem. Phys.* **97**, 7590–7599.
Wójcik, G., Giermańska, J., Marqueton, Y. & Ecolivet, C. (1991). *J. Raman Spectrosc.* **22**, 375–381.
Wójcik, G. & Holband, J. (2001). *Acta Cryst.* B**57**, 346–352.
Wójcik, G. & Holband, J. (2002). *Acta Cryst.* B**58**, 684–689.
Wójcik, G. & Holband, J. (2003). In preparation.
Wójcik, G., Jakubowski, B., Szostak, M. M., Hołderna-Natkaniec, K., Mayer, J. & Natkaniec, I. (1992). *Phys. Status Solidi*, **134**, 139–150.
Wójcik, G., Lipiński, J., Szostak, M. M. & Komorowska, M. (1996). *Adv. Mater. Opt. Electron.* **6**, 307–311.
Wójcik, G., Szostak, M. M., Misiaszek, T., Pająk, Z., Wąsicki, J., Kołodziej, H. A. & Freundlich, P. (1999). *Chem. Phys.* **249**, 201–213.